



Efficient synthesis of dimethyl carbonate via transesterification of ethylene carbonate over a new mesoporous ceria catalyst



Jie Xu^{a,*}, Kai-Zhou Long^a, Fei Wu^a, Bing Xue^a, Yong-Xin Li^{a,*}, Yong Cao^b

^a Jiangsu Key Laboratory of Advanced Catalytic Materials and Technology, College of Chemistry and Chemical Engineering, Changzhou University, Gehu Road 1, Changzhou, Jiangsu 213164, PR China

^b Shanghai Key Laboratory of Molecular Catalysis and Innovative Materials, Department of Chemistry, Fudan University, Shanghai 200433, PR China

ARTICLE INFO

Article history:

Received 9 May 2014

Received in revised form 21 June 2014

Accepted 6 July 2014

Available online 11 July 2014

Keywords:

Dimethyl carbonate

Ethylene carbonate

Transesterification

Ceria

ABSTRACT

Mesoporous ceria materials ($\text{CeO}_2\text{-meso}$) have been prepared through a soft-templating method using cetyltrimethylammonium bromide as a template and cerium nitrate as a precursor. The synthesized $\text{CeO}_2\text{-meso}$ materials possess narrow pore size distributions of 5.1–5.4 nm and tunable surface areas (109–182 $\text{m}^2 \text{g}^{-1}$). As heterogeneous catalysts in the transesterification of ethylene carbonate (EC) with methanol to dimethyl carbonate (DMC), $\text{CeO}_2\text{-meso}$ materials demonstrate superior catalytic performance to the commercial ceria. N_2 adsorption–desorption and CO_2 -TPD characterization results indicate that the catalytic activity obtained over various $\text{CeO}_2\text{-meso}$ samples depends on their surface areas and basicity. The highest activity is achieved over $\text{CeO}_2\text{-meso-400}$, affording a DMC yield as much as 73.3%, together with excellent recycling ability. Besides the transesterification of EC with methanol, $\text{CeO}_2\text{-meso}$ is found to be able to catalyze the reactions of other cyclic carbonates and alcohols. In view of the high catalytic performance along with the convenience in catalyst preparation, $\text{CeO}_2\text{-meso-400}$ compares favorably with the ionic liquids as well as other ceria-based catalytic systems.

© 2014 Elsevier B.V. All rights reserved.

1. Introduction

Dimethyl carbonate (DMC) has been used for a variety of applications in the chemical industries owing to its versatile chemical reactivity and unique physical properties [1,2]. It is a potential additive to fuel oil because of its high octane number and rapid biodegradability [3,4]. More importantly, DMC is an environmentally friendly and promising alternative to highly toxic phosgene and conventional dimethyl sulfate in carbonylation and methylation reactions, respectively [5,6]. Traditionally, DMC is synthesized via the phosgenation or oxidative carbonylation of CH_3OH , which involves high-risk compounds including COCl_2 and CO [7,8]. To circumvent this issue, much effort has been devoted to the direct manufacture of DMC from CO_2 and CH_3OH in the presence of organometallic complexes, inorganic bases, etc. Unfortunately, due to the high inertness of CO_2 as well as the thermodynamic limitations, the DMC yield of the process is relatively low [9–11].

The transesterification of cyclic carbonate (e.g. ethylene carbonate (EC) or propylene carbonate (PC)) with CH_3OH has been regarded as a clean and sustainable synthetic route for the

production of DMC (Scheme S1) [10,12], since cyclic carbonates can be synthesized in a quantitative yield via cycloaddition of CO_2 to epoxides [10]. Furthermore, the co-products obtained in the transesterification, i.e. ethylene glycol (EG) and propylene glycol (PG), are also important industrial reagents [13]. A wide range of heterogeneous catalysts, including basic metal oxides [14], alkali-metal hydroxide [15], anion-exchange resin [16], hydrotalcite [17], dawsonite [18], smectite [19], mesoporous carbon nitride [20], etc., have been developed for the transesterification reactions. Up to now, the most efficient catalysts proposed for the process have been confined to ionic liquids (ILs) [4,21]. However, the thorny issue associated with such ILs is the catalyst–product separation [22]. Although immobilization the ILs onto solid support (e.g. porous silica materials) can solve this problem, the high cost of siliceous coupling agents and tedious preparation for the immobilized ILs still restrict their practical applications [20]. In this context, it is highly desired to develop a new catalyst that can allow a robust activity along with easy separation for the transesterification reactions.

Ceria is one of the most important rare earth oxides. As a key redox component, ceria has been extensively used in for many catalytic processes [23], such as three-way-catalyst for exhaust treatment, low-temperature CO oxidation [24], and water-gas shift [25]. Moreover, ceria is also a typical Lewis-base catalyst, which is

* Corresponding authors. Tel.: +86 519 86330135.

E-mail addresses: shine6832@163.com (J. Xu), liyxluck@163.com (Y.-X. Li).

responsible for its application in several base-catalyzing processes. Tomishige et al. [26] have reported the utilization of high-surface-area ceria ($40\text{--}131\text{ m}^2\text{ g}^{-1}$) for the direct synthesis of organic carbonate from the reaction of CO_2 with CH_3OH . Wherein, the catalytically active sites were attributed to the (1 1 1) faces of ceria. Adopting SBA-15 as a hard template through a nanocasting pathway, Liu et al. [27] have prepared a series of mesoporous ceria ($S_{\text{BET}} = 135\text{ m}^2\text{ g}^{-1}$) catalysts loaded with NaOH/KOH . As a superbase, the synthesized mesoporous ceria material showed excellent catalytic performance (DMC yield = 65%) in transesterification of EC with CH_3OH at 65°C . Corma et al. [28] also revealed that cerias loaded with nanosized gold could promote the transesterification of PC with CH_3OH to DMC at 140°C , affording a maximum DMC yield of 35%. Also, ceria-based mixed oxides (e.g. $\text{MgO}\text{-CeO}_2$ [29]) have been reported to be able to catalyze the transesterification of cyclic carbonates.

The effort above has verified the catalytic capability of ceria for the transesterification reactions of cyclic carbonates to DMC. In the continued search for a more effective ceria for the transesterification of cyclic carbonates to DMC, there is a definite demand for an economic and facile method for the preparation of ceria that can allow efficient activity for the production of DMC. In our previous work [30], we reported the synthesis of mesoporous ceria materials using a soft-templating approach, which showed potential catalytic application for the oxidative dehydrogenation of ethylene benzene to styrene. Herein, we employ the mesoporous ceria catalyst ($\text{CeO}_2\text{-meso}$) as a new catalyst for the transesterification reaction of cyclic carbonates and alcohol. The $\text{CeO}_2\text{-meso}$ materials exhibit high and steady activity in the transesterification of EC with CH_3OH . Based on the characterization results of N_2 adsorption–desorption and CO_2 -TPD, the high surface area and the abundant basicity are responsible for its high catalytic activity. Besides EC, $\text{CeO}_2\text{-meso}$ could also promote a series of transesterification of other cyclic carbonates.

2. Experimental

2.1. Catalyst preparation

Mesoporous ceria materials were synthesized via a template-assisted precipitation method [30,31]. Typically, 4.34 g $\text{Ce}(\text{NO}_3)_3\text{-}6\text{H}_2\text{O}$ was added into 200 mL of 0.03 mol L^{-1} solution of cetyltrimethylammonium bromide ($\text{C}_{16}\text{H}_{33}\text{N}(\text{CH}_3)_3\text{Br}$, CTAB), and stirred vigorously for 3 h. Next, a NaOH solution (2 g in 300 mL of water) was added into the above solution and then stirred overnight. After that, the mixture was transferred into an autoclave and aged at 90°C for 12 h. The as-received yellow precipitate was filtered and washed with hot water (ca. 80°C) for several times to remove the residual CTAB. The resultant yellow powder was dried at 110°C for 6 h and then calcined for 4 h. The resultant ceria samples are denoted as $\text{CeO}_2\text{-meso-}T$, where T stands for the calcination temperature.

2.2. Sample characterization

X-ray diffraction patterns were recorded with a Rigaku D/max 2500 PC X-ray diffractometer equipped with a graphite monochromator (40 kV, 40 mA) using Ni-filtered $\text{Cu-K}\alpha$ radiation ($\lambda = 1.5418\text{\AA}$).

Nitrogen adsorption–desorption isotherms were measured at -196°C using a Micromeritics ASAP 2020 analyzer. Prior to the analysis, the samples were degassed ($1.33 \times 10^{-2}\text{ Pa}$) at 150°C for at least 4 h. The specific surface area was calculated according to the Brunauer–Emmet–Teller (BET) method, and pore size distribution was determined by the Barret–Joyner–Halenda method.

Transmission electron microscopy (TEM) experiments were conducted on a JEOL 2010 electron microscope operating at 200 kV. Before being transferred into the TEM chamber, the samples dispersed in ethanol were deposited onto holey carbon films supported on Cu grids.

Diffused reflection infrared Fourier transform (DRIFT) spectra were collected using a Bruker Tensor 27 spectrometer. The samples were placed in in-situ cell and pretreated with heating at 200°C for 1 h under N_2 flow.

The basicity of the samples was measured by CO_2 temperature-programmed desorption ($\text{CO}_2\text{-TPD}$) on a Quantachrome ChemBET-3000 analyzer. A 200 mg of the sample was pretreated at 300°C for 1 h in dry He flow (30 mL min^{-1}), cooled to 50°C , and then exposed to CO_2 for 0.5 h. After purging the sample with He for 0.5 h, the TPD data was recorded from 50 to 550°C with a ramping rate of $10^\circ\text{C min}^{-1}$.

2.3. Catalytic test

The transesterification reactions of EC with CH_3OH were carried out in 80 mL stainless steel autoclave equipped with a magnetic stirrer. 25 mmol of EC and 250 mmol of CH_3OH were mixed well, followed by the introduction of 0.1 g of the catalyst. The reactor was pressurized with CO_2 to 0.6 MPa and heated to 140°C under stirring for 2 h. After the reaction, the autoclave was cooled down in ice water and the mixture was centrifuged and analyzed by a GC equipped with a PEG-2000 capillary column coupled with a FID detector. The quantity of reagents and products are calculated by an area-normalization method. The carbon balance was $100 \pm 5\%$. In the transesterification of EC with CH_3OH , DMC and 2-hydroxyethyl methyl carbonate (HEMC) is the target molecule and by-product, respectively. The glycol is co-product. The conversion (Conv.) of EC and selectivity (Sel.) to DMC are calculated as follows:

$$\text{Conv.\%} = \frac{n_{\text{EC,fed}} - n_{\text{EC,uncovered}}}{n_{\text{EC,fed}}}, \text{ and Sel.\%} = \frac{n_{\text{DMC}}}{n_{\text{EC,fed}} - n_{\text{EC,uncovered}}}$$

The filtered catalyst was washed with methanol (50 mL) for two times, dried overnight, and then investigated for its next running. The catalytic activity for each catalyst is based on its specific reaction rate (r_s , $\text{g EC g catalyst}^{-1} \text{ h}^{-1}$), which is calculated as follows:

$$r_s = \frac{m_{\text{EC,converted}}}{W_{\text{catal.}} \times t} = \frac{n_{\text{EC}} \times \text{Conv.\%}(EC) \times M_{\text{EC}}}{W_{\text{catal.}} \times t}$$

where n_{EC} , M_{EC} , t , and $W_{\text{catal.}}$ are the molar amount (mol), formula weight (88 g mol^{-1}) of EC, reaction time (h), and the mass of the catalyst (g), respectively.

3. Results and discussion

3.1. Catalyst characterization

XRD patterns of the commercial and mesoporous ceria samples are shown in Fig. 1. All samples present intensive diffraction peaks at $2\theta = 28.5^\circ$, 33.1° , 47.46° , and 56.3° , corresponding to the characteristic diffractogram of cubic fluorite structure (JCPDS: 34-0394). The commercial ceria shows very strong and sharp diffraction lines. Calculated by Scherrer equation based on the (1 1 1) plane, the crystallite size of $\text{CeO}_2\text{-com}$ is ca. 54.7 nm (Table 1). By contrast, the diffraction peaks acquired over $\text{CeO}_2\text{-meso}$ materials are broader and weaker than $\text{CeO}_2\text{-com}$, suggesting that the average particle sizes of ceria are rather small. As the calcination temperature increases from 400 to 600°C , the diffraction peaks become sharper, indicating that the crystallinity is improved. Meanwhile, the corresponding crystallite sizes of cerias, calculated by Scherrer's equation (based on the (1 1 1) plane), increase from 8.8 to 9.5 nm as the annealing temperature is raised from 400 to 600°C .

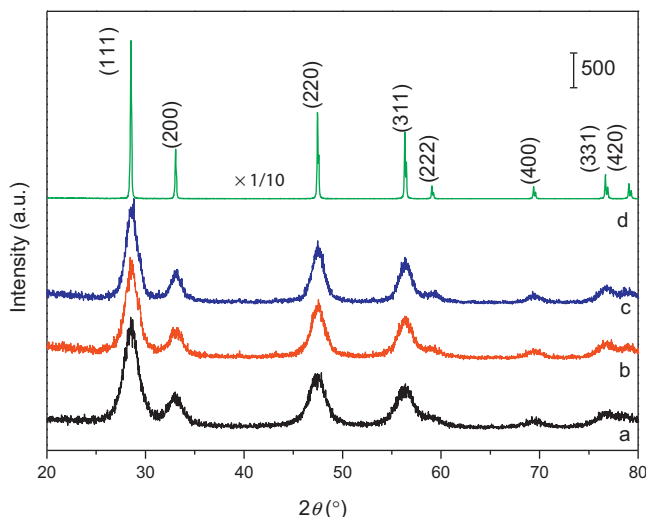


Fig. 1. XRD patterns of CeO_2 -meso-T (400–600: a–c) and CeO_2 -com (d) materials.

The XRD information obtained over the mesoporous ceria materials are similar to the mesoporous ceria materials synthesized via hard templating routes [27,32], and cerias with other shapes [33] reported previously.

Fig. 2A depicts the N_2 adsorption–desorption isotherms of CeO_2 -meso materials with different calcination temperatures. The three samples demonstrate apparent type IV curves with H1 hysteresis loops at $p/p_0 = 0.55\text{--}0.85$. Meanwhile, in the range of high pressure, i.e. $p/p_0 > 0.90$, no evident N_2 adsorption has been observed, suggesting that the CeO_2 -meso materials possess exclusive mesostructures. In the case of CeO_2 -com, the quantity of N_2 adsorbed is very low ($<3 \text{ cm}^3 \text{ g}^{-1}$ (STP), not shown here), which means that its pore structures are very poor. The corresponding pore size distribution (PSD) curves are shown in Fig. 2B. The PSDs for the CeO_2 -meso samples do not differ significantly; all exhibit mesopores centered at 5.0–5.5 nm with a narrow distribution. The textual parameters of various ceria samples are summarized in Table 1. In sharp contrast to the commercial ceria with a poor

Table 1
Textural parameters of ceria samples.

Sample	$S_{\text{BET}} (\text{m}^2 \text{ g}^{-1})$	$D_{\text{pore}} (\text{nm})$	$V_{\text{pore}} (\text{cm}^3 \text{ g}^{-1})$	$D_{\text{particle}} (\text{nm})^{\text{a}}$
CeO_2 -meso-400	182	5.41	0.249	8.8
CeO_2 -meso-500	149	5.29	0.226	9.3
CeO_2 -meso-600	109	5.18	0.179	9.5
CeO_2 -com	4	—	<0.01	54.7
CeO_2 -meso-400 ^b	171	5.30	0.246	8.9

^a Calculated based on the (1 1 1) planes.

^b Spent catalyst after five consecutive runs.

porosity, CeO_2 -meso materials possess considerably higher BET surface areas as well as larger pore volumes. With the increase of calcination temperature from 400 to 600 °C, the surface areas and pore volumes decrease gradually. This is mainly attributed to the agglomeration of ceria nanoparticles and/or partial shrinkage of mesostructures occurring at higher calcination temperature, which has been verified by the corresponding structural values listed in Table 1.

The mesoporous structures of ceria materials were further investigated by TEM and a representative image of CeO_2 -meso-400 is shown in Fig. 3. The image reveals that the ceria is composed of nanoparticles, which are 7–9 nm sized, consistent with the crystallite size calculated by XRD characterization results. Moreover, foam-like mesopores can be also observed in the image, especially at the edge of the sample. The TEM image indicates that the mesopores of CeO_2 -meso mainly arise from the nanosized channels among the nanoparticles.

Furthermore, we have also prepared a ceria sample annealed at lower temperature (300 °C). The N_2 adsorption–desorption isotherm and its corresponding textual parameters are provided in Fig. S1, and Table S1, respectively. Although the surface area of such CeO_2 -meso-300 ($192 \text{ m}^2 \text{ g}^{-1}$) is very close to that of CeO_2 -meso-400, the pore size is only 4.3 nm, ca. 20% less than the value acquired over other CeO_2 -meso samples. As mentioned above, the present mesoporous ceria materials are fabricated via the soft templating method using CTAB as the template. Unlike polyether surfactants, such as nonionic P123 employed in the preparation of SBA-15 [34], the CTAB molecule has substantial C instead of O atoms.

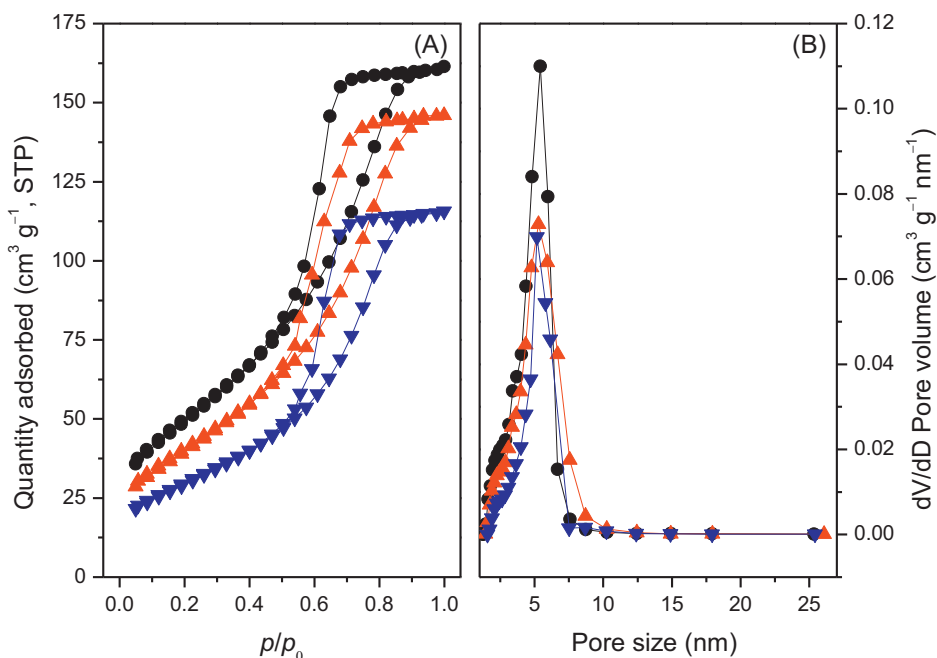


Fig. 2. N_2 adsorption–desorption isotherms (A) and pore size distributions (B) of CeO_2 -meso-T (●: 400; ▲: 500; ▼: 600) materials.

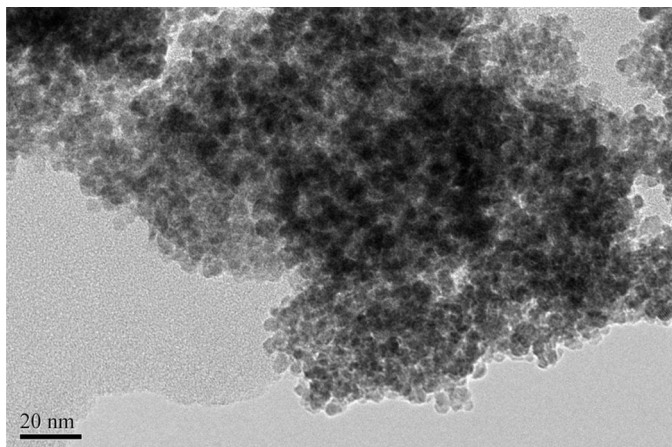


Fig. 3. TEM image of CeO₂-meso-400.

Simultaneously, the interaction between CTAB and inorganic Ce species is electrostatic force [35], generally stronger than the hydrogen bond between P123 and silicate compounds. Therefore, to eliminate CTAB, washing procedure with hot water was conducted after the hydrothermal step. Despite this, there were still some CTAB molecules remaining in the as-synthesized ceria materials. As shown in Fig. S2, the pure CTAB reveals a sharp weight loss (ca. 97 wt%) in the range of 200–350 °C. Obviously, this is attributed to the decomposition of CTAB in air. In the case of the as-synthesized CeO₂ before calcination, it also demonstrates an apparent weight loss in the same temperature range, contributing to ca. 9 wt% of overall weight. On the other hand, the synthesized CeO₂-meso shows no significant weight loss (ca. 0.5 wt%) at ca. 200–350 °C. The comparison strongly verifies the existence of residual CTAB in the as-synthesized CeO₂ sample. In this sense, the introduction of subsequent calcination plays a crucial role to obtain mesoporous ceria with high surface area. First, the temperature value ought to be higher than the decomposition temperature (ca. 350 °C) of CTAB, thus guaranteeing the complete elimination of CTAB. A low calcination temperature is inevitably unfavorable to remove the template, resulting in a lower pore size and poor crystallinity (Fig. S3), compared with those of CeO₂-meso samples prepared using high calcination temperatures. Second, calcination is also necessary for the crystallization from the amorphous ceria to cubic fluorite structure. Third, the temperature should not be too high; higher temperatures would induce inevitable aggregation of ceria nanoparticles and consequent decrease in surface areas and pore volumes of the final mesoporous ceria materials.

The basicity of the mesoporous ceria samples was analyzed using CO₂-TPD measurement. As displayed in Fig. 4, all mesoporous samples exhibit broad desorption peaks centered at ca. 145 °C, attributed to the basic sites associated with weak chemical and/or physical adsorption of acidic CO₂ molecules. In contrast, CeO₂-com gives a weak TCD signal of CO₂ adsorbed, indicating that the basic species in it are very scarce. Moreover, based on the peak areas integrated, the density of the base sites for CeO₂-meso-400 is 212 μmol CO₂ g_{catal.}⁻¹. Upon increasing the calcination temperature, the basic quantity decreases. This variation is in good agreement with the finding in terms of surface areas described above. On the other hand, the difference between the CeO₂-com and CeO₂-meso probably originates from their significant distinction in terms of the textual properties. Wherein, high surface areas along with mesoporous architecture would offer abundant exposed basic sites as well as favorable mass transfer in the CO₂-TPD analysis.

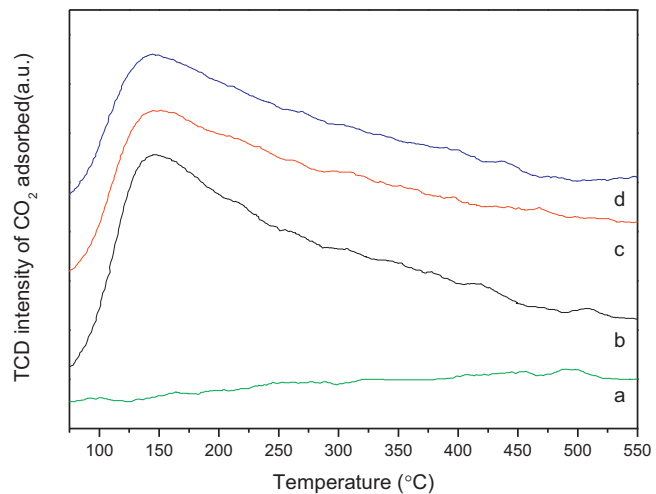


Fig. 4. CO₂-TPD profiles of CeO₂-com (a), CeO₂-meso-400 (b), CeO₂-meso-500 (c), and CeO₂-meso-600 (d) materials.

3.2. Catalyst activity

Initially, a blank experiment without catalyst was carried out for the transesterification of EC with CH₃OH (entry 1, Table 2). The result reveals that the reaction can proceed with a minor conversion under such circumstance, affording an EC conversion of 18.0%. Wherein, the monoester, namely HEMC, accounts for a large proportion in the products. After the introduction of CeO₂-com, the catalytic conversion is slightly enhanced (entry 2). Upon employing the CeO₂-meso catalyst, the conversion increases drastically, together with a high selectivity (96.1%) to the target molecule, DMC. Additionally, the variation of catalytic performances obtained over different mesoporous ceria sample has been found. As listed in entries 3–5, the catalytic activity of CeO₂-meso decreases monotonously with the increase of their corresponding calcination temperatures, and the prominent activity is achieved over CeO₂-meso-400, which offers the highest EC yield of 73.3%.

As stated above, it has been reported that ceria can catalyze the esterification of CO₂ with CH₃OH to DMC [26]. To examine the possible contribution of the catalytic esterification to the present transesterification system of EC with CH₃OH, we also tested the esterification reaction over CeO₂-meso without the addition of EC. The result (entry 6) confirms that, under the present reaction circumstance, CeO₂-meso could hardly promote the esterification of CO₂ with CH₃OH. That is, the DMC gained in the study solely results from the transesterification of EC with CH₃OH. In addition to the high-temperature evaluation, the catalytic behavior under a low

Table 2
Catalytic performances of ceria catalyst in the transesterification reaction of EC with CH₃OH.

Entry	Catalyst	Conv. (%)	Sel. (%)		Yield (%)
			DMC	HEMC	
1	— ^a	18.0	46.2	53.8	8.3
2	CeO ₂ -com ^a	23.6	50.3	49.7	11.9
3	CeO ₂ -meso-400 ^a	76.3	96.1	3.9	73.3
4	CeO ₂ -meso-500 ^a	67.4	94.7	5.3	63.8
5	CeO ₂ -meso-600 ^a	60.8	93.9	6.1	57.1
6	CeO ₂ -meso-400 ^b	—	—	—	Trace
7	— ^c	21.5	17.2	82.8	3.7
8	CeO-com ^c	36.3	37.8	62.2	13.7
9	CeO-meso-400 ^c	43.2	77.7	22.3	33.6

^a 250 mmol of CH₃OH, 25 mmol of EC, T = 140 °C, W_{catal.} = 0.1 g, and t = 2 h.

^b 250 mmol of CH₃OH, T = 140 °C, W_{catal.} = 0.1 g, and t = 2 h.

^c 250 mmol of CH₃OH, 25 mmol of EC, T = 70 °C, W_{catal.} = 0.2 g, and t = 12 h.

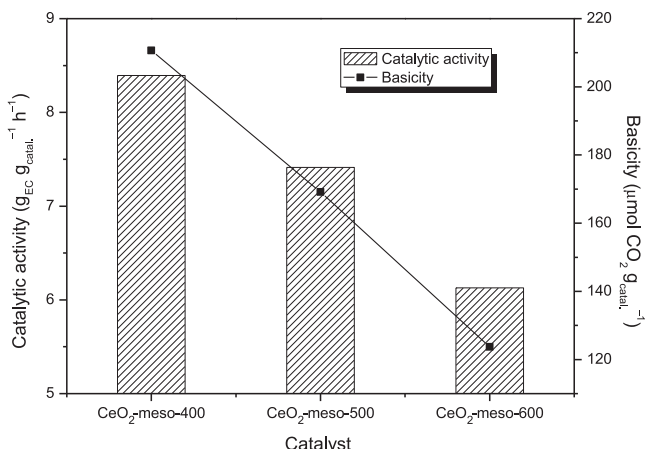


Fig. 5. Correlation between the catalytic activity and the basicity in $\text{CO}_2\text{-TPD}$ profiles of various ceria catalysts.

temperature has also been surveyed. At 70°C and reaction time for 12 h, $\text{CeO}_2\text{-com}$ catalyzes the reaction of EC with CH_3OH with a moderate EC conversion and the DMC selectivity is very low (entry 8). Under the same reaction condition, its mesoporous counterpart provides a higher catalytic conversion and remarkable selectivity (77.7%). Combining the catalytic performance in high and low temperature, it can be seen that the mesoporous ceria materials can catalyze the transesterification of EC with CH_3OH with high activities.

To gain further insight into the basic property of the mesoporous ceria catalysts in relation to their activity in the transesterification, the basicity intensity based on the $\text{CO}_2\text{-TPD}$ results is plotted against the catalytic activity ($\text{g}_{\text{EC}} \text{ converted g}_{\text{catal.}}^{-1} \text{ h}^{-1}$) for the $\text{CeO}_2\text{-meso-400/500/600}$ sample. As depicted in Fig. 5, the basicity intensity exhibits a good correlation with its corresponding catalytic activity. Moreover, considering the variation of the three mesoporous ceria samples in terms of their textual properties, the basicity intensity for each $\text{CeO}_2\text{-meso}$ is further calculated regarding the surface area. The resultant intensity for $\text{CeO}_2\text{-meso-400/500/600}$ is $1.15, 1.13, 1.13 \mu\text{mol CO}_2 \text{ m}^{-2}$, which are fairly close. Thus, it can be confirmed again that the variation of the basicity of the mesoporous CeO_2 materials originates from their surface areas. On the other hand, it is widely reported that ceria is a typically amphoteric metal oxide, featuring both acid and base nature [36], and the transesterification reactions can also be promoted by either acid or base. Therein, to examine the possible involvement of acid property for the transesterification in the present mesoporous ceria catalyst, we have also used $\text{NH}_3\text{-TPD}$ measurement (see supporting information for the detailed experiment) to probe the acidity of the three $\text{CeO}_2\text{-meso}$ samples above. As shown in Fig. S4, there is no apparent relevance between the acid density and the catalytic activity in the mesoporous CeO_2 materials. Based on the $\text{CO}_2/\text{NH}_3\text{-TPD}$ profiles above, it can be concluded that the basic sites of $\text{CeO}_2\text{-meso}$ contributes directly to the activity in the transesterification of EC with CH_3OH .

In order to elucidate the dependence of the catalytic performance on the reaction conditions, the catalytic conversions and selectivities at different reaction time and temperatures have been investigated. At the first 0.5 h, the reaction proceeds with a moderate EC conversion as much as 46.6%, and the selectivity to DMC received is 72.8% (Fig. 6A). As the reaction is prolonged, the conversion and selectivity increase progressively but level off after 2 h. On the other hand, the reaction temperature also exhibits a noticeable relationship with the catalytic performance

of the transesterification. As shown in Fig. 6B, both conversion and selectivity undergo a notable enhancement in the range of $100\text{--}140^\circ\text{C}$. In particular, the temperature of 120°C is found to be a critical threshold in gaining a high content of DMC. Since the reaction of EC with CH_3OH essentially involves two-step of transesterification ($\text{EC} + \text{CH}_3\text{OH} \rightarrow \text{HEMC} \rightarrow \text{DMC}$), mild reaction conditions such as low temperature and/or short time easily impede the occurrence of the second stage. Consequently, a low selectivity to the desired DMC would be received. This phenomenon has also been reported in transesterification of EC over other catalytic systems [3,4,20]. Given the results above, a temperature of 140°C and reaction time of 2 h were chosen as optimal reaction conditions.

Besides the reaction time and temperature, another issue of practical importance for the evaluation of a heterogeneous catalyst is the recycling capability. In view of this, a series of consecutive experiments have been performed. As described in Fig. S5, the selectivity in each cycle is above 96%. As for the conversion, no apparent loss ($\pm 5\%$) has been observed during the five repetitive runs. N_2 adsorption–desorption and FT-IR techniques were further employed to analyze the physiochemical properties of the used $\text{CeO}_2\text{-meso-400}$ catalyst subjected to five runs. The surface area and pore size of the spent $\text{CeO}_2\text{-meso-400}$ are $171 \text{ m}^2 \text{ g}^{-1}$ and 5.30 nm , respectively (Table 1 and Fig. S6). Moreover, the XRD pattern demonstrates no clear change in the crystallinity compared with the fresh $\text{CeO}_2\text{-meso-400}$ sample (Table 1). In the case of chemical composition, the fresh and spent ceria samples show identical DRIFT spectra (Fig. S7). The bands at ca. 3660 and 3550 cm^{-1} are attributed to the O–H stretching modes of bridged OH on the ceria [26], and adsorbed water, respectively. The strong peak at ca. 660 cm^{-1} is due to the stretching frequency of Ce–O–Ce [37]. In addition, the bands in the frequency region from 1200 to 1700 cm^{-1} are assigned to carbonate species formed by coordination of CO_2 molecules onto the coordinatively unsaturated CeO_2 surface [38]. Obviously, no band associated with the reagent/product of the transesterification reaction has been discovered. Therein, the steady textual and chemical properties are responsible for the excellent reproducibility of the mesoporous ceria catalyst.

In addition to the transesterification reaction of EC with CH_3OH , the reaction between PC and CH_3OH has also been tested in the presence of $\text{CeO}_2\text{-meso-400}$ (Table 3). The result (entry 2) indicates that the catalytic reaction undergoes with a minor conversion. Generally, the transesterification of cyclic carbonate is a typical nucleophilic addition reaction that can be catalyzed by either acid or base. In the previous work, the basic hydroxyl (Ce–O–H) groups has been recognized as the key site to adsorb and activate CH_3OH molecules [26], yielding highly active CH_3O^- anion. Due to the steric hindrance, the nucleophilic addition of the anion to PC is more difficult than EC and consequently lower yield is obtained in the transesterification of PC. Nevertheless, prolonging the reaction or elevating the temperature can facilitate the catalytic transesterification of PC with CH_3OH (entries 3 and 4) and then receive a higher conversion. Furthermore, EC and PC can also be catalytically transesterified with $\text{C}_2\text{H}_5\text{OH}$ over $\text{CeO}_2\text{-meso-400}$ (entries 5 and 6) at 160°C .

Table 4 compares the performances of various representative catalysts, including ILs and ceria-based materials. Note, for a fair comparison, all the performances collected are based on the batch reactor. The best catalytic activities were achieved over ILs (entries 1–4). Especially, DMIC afforded a top activity as much as $38.75 \text{ g}_{\text{EC}} \text{ g}_{\text{catal.}}^{-1} \text{ h}^{-1}$ at 110°C , and the performance was largely owing to the intrinsically homogeneous nature that is beneficial to the contact of active sites with the substrates. However, as discussed above, the main drawback for such IL-catalyzed system lies in the inconvenience in the separation of

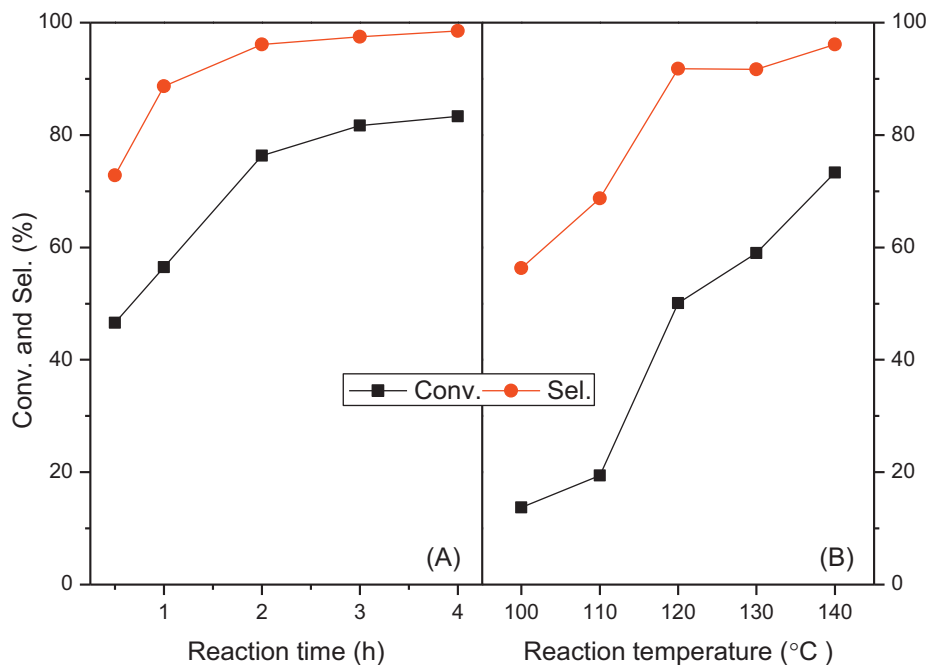


Fig. 6. Effect of reaction time (A) and temperature (B) on the transesterification over CeO_2 -meso-400 catalyst. Reaction conditions: 250 mmol of CH_3OH , 25 mmol of EC, and $W_{\text{catal.}} = 0.1 \text{ g}$.

the catalysts. Furthermore, the supported ILs (entries 5 and 6) suffer from high-cost and complicated immobilization procedure. As far as ceria-based catalysts concerned, although the NaMC and Au/CeO_2 demonstrate superior activity to CeO_2 -meso, the synthetic routes associated with the two ceria-based samples is complex. In sharp contrast, the present CeO_2 -meso materials are fabricated via

a soft-templating approach which is facile, simple and cheap. More importantly, no further loading is demanded. At this juncture, the comparison in Table 4 strongly suggests that the single CeO_2 -meso catalyst, featuring low-cost preparation and high catalytic activity, can serve as a promising heterogeneous catalyst for the synthesis of DMC via transesterification of EC with CH_3OH .

Table 3

Catalytic performance of CeO_2 -meso-400 in various transesterification of cyclic carbonates with alcohols ^a.

Entry	Cyclic carbonate	Alcohol	T (°C)	t (h)	Conv. (%)	Sel. (%) ^b	Yield (%)
1	EC	CH_3OH	140	2	76.3	96.1	73.3
2	PC	CH_3OH	140	2	18.0	91.9	16.5
3	PC	CH_3OH	140	6	37.5	98.6	37.0
4	PC	CH_2OH	160	6	59.8	99.2	59.3
5	EC	$\text{C}_2\text{H}_5\text{OH}$	160	6	80.6	92.5	74.5
6	PC	$\text{C}_2\text{H}_5\text{OH}$	160	6	34.0	97.9	33.3

^a Reaction condition: 250 mmol of alcohol, 25 mmol of cyclic carbonate, $W_{\text{catal.}} = 0.1 \text{ g}$.

^b The sole byproduct is monoester.

Table 4

Comparison of the catalytic performances of ILs and ceria-based catalysts for the transesterification of EC with CH_3OH to DMC.^a

Entry	Catalyst	$W_{\text{catal.}}$ (g)	n_{EC} (mmol)	$n_{\text{CH}_3\text{OH}}/n_{\text{EC}}$	T (°C)	t (h)	EC conv. (%)	r_s ($\text{g}_{\text{EC}} \text{g}_{\text{catal.}}^{-1} \text{h}^{-1}$)
1	[BmIm]Cl [21] ^b	0.348	25	5:1	140	6	74.1	0.78
2	[BmIm]Cl [7] ^{b,c}	0.348	25	8:1	120	0.25	59.1	14.94
3	DABCO-derived IL [3] ^d	0.0187	10	15:1	70	6	90	7.06
4	DMIC [4] ^e	0.028	20	10:1	110	1.33	82	38.75
5	IL on MCM-41 [39] ^f	0.2	25	8:1	180	4	78.4	2.16
6	MCF-[SmIm]OH [13] ^g	0.5	32	10:1	65	5	85	0.96
7	NaMC [27] ^h	0.08	100	5:1	65	3	64.5	23.65
8	Au/CeO_2 [28] ⁱ	0.115	10	10:1	140	6	63	0.80
9	CeO_2 -meso-400	0.1	25	10:1	140	2	76.3	8.4

^a Unless specified, the reactions with temperatures over 70 °C were carried out in an autoclave under CO_2 atmosphere (0.5–1.2 MPa).

^b [BmIm]Cl: 1-*n*-butyl-3-methylimidazolium.

^c Microwave (100 W) heating.

^d DABCO: 1-*n*-butyl-1,4-diazabicyclo[2.2.2]octane.

^e DMIC: 1,3-dimethylimidazolium-2-carboxylate.

^f IL: 1-(triethoxysilyl) propyl-tri-*n*-hexylammonium chloride.

^g [SmIm]OH: 1-(triethoxysilyl) propyl-3-methylimidazolium hydroxide.

^h Mesoporous ceria loaded with NaOH.

ⁱ Transesterification of PC with CH_3OH .

4. Conclusion

In summary, high-surface area ceria materials ($109\text{--}182\text{ m}^2\text{ g}^{-1}$) with pore sizes of $5.1\text{--}5.4\text{ nm}$ have been synthesized via a soft-templating method using CTAB as a template. The mesoporous ceria materials are new heterogeneous catalysts applicable for the synthesis of DMC from transesterification of EC. The catalytic activities of CeO_2 -meso samples are highly dependent on their textual and basicity properties. CeO_2 -meso-400 offers the highest EC conversion of 76% with an excellent DMC selectivity of 96% and demonstrates stable recyclability. The active sites of CeO_2 have been specified as the base rather than acid. In addition, the mesoporous ceria can also catalyze the transesterification PC with $\text{CH}_3\text{OH}/\text{C}_2\text{H}_5\text{OH}$ with moderate conversions. Compared with the previously reported ILs and other ceria-based catalysts, the heterogeneous CeO_2 -meso catalysts have remarkable merits in catalyst preparation, recycling, and catalytic activity. Therefore, it can be inferred that the mesoporous ceria materials are of practical potential for the synthesis of DMC.

Acknowledgments

This work was supported by National Natural Science Foundation of China (21203014), Open Foundation of Jiangsu Key Laboratory of Fine Petrochemical Engineering (KF1201), Jiangsu Key Laboratory of Advanced Catalytic Materials and Technology (BM2012110), and the Project Funded by the Priority Academic Program Development of Jiangsu Higher Education Institutions.

Appendix A. Supplementary data

Supplementary material related to this article can be found, in the online version, at <http://dx.doi.org/10.1016/j.apcata.2014.07.009>.

References

- [1] P. Tundo, M. Selva, *Acc. Chem. Res.* 35 (2002) 706–716.
- [2] M. Sankar, S. Satav, P. Manikandan, *ChemSusChem* 3 (2010) 575–578.
- [3] Z.-Z. Yang, L.-N. He, X.-Y. Dou, S. Chanfreau, *Tetrahedron Lett.* 51 (2010) 2931–2934.
- [4] J.-Q. Wang, J. Sun, W.-G. Cheng, C.-Y. Shi, K. Dong, X.-P. Zhang, S.-J. Zhang, *Catal. Sci. Technol.* 2 (2012) 600–605.
- [5] B.M. Bhanage, S. Fujita, Y. Ikushima, M. Arai, *Green Chem.* 5 (2003) 429–432.
- [6] Y. Ono, *Catal. Today* 35 (1997) 15–25.
- [7] M.M. Dharman, H.-Y. Ju, H.-L. Shim, M.-K. Lee, K.-H. Kim, D.-W. Park, *J. Mol. Catal. A* 303 (2009) 96–101.
- [8] Y. Ding, A. Kong, H. Zhang, H. Shen, Z. Sun, S.D. Huang, Y. Shan, *Appl. Catal. A* 455 (2013) 58–64.
- [9] L. Wang, Y. Wang, S. Liu, L. Lu, X. Ma, Y. Deng, *Catal. Commun.* 16 (2011) 45–49.
- [10] S.R. Jagtap, M.D. Bhor, B.M. Bhanage, *Catal. Commun.* 9 (2008) 1928–1931.
- [11] W.-L. Dai, S.-L. Luo, S.-F. Yin, C.-T. Au, *Appl. Catal. A* 366 (2009) 2–12.
- [12] T. Wei, M. Wang, W. Wei, Y. Sun, B. Zhong, *Green Chem.* 5 (2003) 343–346.
- [13] J. Xu, H.-T. Wu, C.-M. Ma, B. Xue, Y.-X. Li, Y. Cao, *Appl. Catal. A* 464–465 (2013) 357–363.
- [14] H. Wang, M. Wang, S. Liu, N. Zhao, W. Wei, Y. Sun, *J. Mol. Catal. A* 258 (2006) 308–312.
- [15] M.S. Han, B.G. Lee, B.S. Ahn, K.Y. Park, S.I. Hong, *React. Kinet. Catal. Lett.* 73 (2001) 33–38.
- [16] S.M. Dhuri, V.V. Mahajani, *J. Chem. Technol. Biotechnol.* 81 (2006) 62–69.
- [17] Y. Watanabe, T. Tatsumi, *Micropor. Mesopor. Mater.* 22 (1998) 399–407.
- [18] G. Stoica, S. Abelló, J. Pérez-Ramírez, *Appl. Catal. A* 365 (2009) 252–260.
- [19] B.M. Bhanage, S.-I. Fujita, Y. He, Y. Ikushima, M. Shirai, K. Torii, M. Arai, *Catal. Lett.* 83 (2002) 137–141.
- [20] J. Xu, K.-Z. Long, T. Chen, B. Xue, Y.-X. Li, Y. Cao, *Catal. Sci. Technol.* 3 (2013) 3192–3199.
- [21] H.Y. Ju, M.D. Manju, D.W. Park, Y. Choe, S.W. Park, *React. Kinet. Catal. Lett.* 90 (2007) 3–9.
- [22] M.H. Valkenberg, D. deCastro, W.F. Holderich, *Green Chem.* 4 (2002) 88–93.
- [23] A. Trovarelli, C. de Leitenburg, M. Boaro, G. Dolcetti, *Catal. Today* 50 (1999) 353–367.
- [24] X.-S. Huang, H. Sun, L.-C. Wang, Y.-M. Liu, K.-N. Fan, Y. Cao, *Appl. Catal. B* 90 (2009) 224–232.
- [25] Q. Fu, H. Saltsburg, M. Flytzani-Stephanopoulos, *Science* 301 (2003) 935–938.
- [26] Y. Yoshida, Y. Arai, S. Kado, K. Kunimori, K. Tomishige, *Catal. Today* 115 (2006) 95–101.
- [27] T.-T. Li, L.-B. Sun, L. Gong, X.-Y. Liu, X.-Q. Liu, *J. Mol. Catal. A* 352 (2012) 38–44.
- [28] R. Juárez, A. Corma, H. García, *Green Chem.* 11 (2009) 949–952.
- [29] H. Abimanyu, C.S. Kim, B.S. Ahn, K.S. Yoo, *Catal. Lett.* 118 (2007) 30–35.
- [30] J. Xu, L.-C. Wang, Y.-M. Liu, Y. Cao, H.-Y. He, K.-N. Fan, *Catal. Lett.* 133 (2009) 307–313.
- [31] M.F. Luo, J.M. Ma, J.Q. Lu, Y.P. Song, Y.J. Wang, *J. Catal.* 246 (2007) 52–59.
- [32] J. Roggenbuck, H. Schäfer, T. Tsioncheva, C. Minchev, J. Hanss, M. Tiemann, *Micropor. Mesopor. Mater.* 101 (2007) 335–341.
- [33] H.-X. Mai, L.-D. Sun, Y.-W. Zhang, R. Si, W. Feng, H.-P. Zhang, H.-C. Liu, C.-H. Yan, *J. Phys. Chem. B* 109 (2005) 24380–24385.
- [34] D. Zhao, J. Feng, Q. Huo, N. Melosh, G.H. Fredrickson, B.F. Chmelka, G.D. Stucky, *Science* 279 (1998) 548–552.
- [35] D. Terrible, A. Trovarelli, J. Llorca, C. de Leitenburg, G. Dolcetti, *J. Catal.* 178 (1998) 299–308.
- [36] L. Vivier, D. Duprez, *ChemSusChem* 3 (2010) 654–678.
- [37] S.B. Khan, M. Faisal, M.M. Rahman, A. Jamal, *Sci. Total Environ.* 409 (2011) 2987–2992.
- [38] T. Mokkelbost, I. Kaus, T. Grande, M.-A. Einarsson, *Chem. Mater.* 16 (2004) 5489–5494.
- [39] D.-W. Kim, D.-O. Lim, D.-H. Cho, J.-C. Koh, D.-W. Park, *Catal. Today* 164 (2011) 556–560.